

A novel transversely-isotropic 3D elastic-viscoplastic constitutive law for modeling fiber matrix composites

M. Vogler^{1,a}, F.X.C. Andrade², J.Schöpfer³, S. Kolling^{4,5}, R. Rolfes¹

¹ Leibniz University Hannover, Institute for Structural Analysis, 30167 Hannover, Germany

² Faculty of Engineering, University of Porto, Portugal

³ Daimler AG, Mercedes Benz Werk Hamburg, Mercedesstr. 1, 21079 Hamburg, Germany

⁴ German Institute for Polymers (DKI), Department of Mechanics and Simulation,
Schlossgartenstr. 6, D-64289 Darmstadt, Germany

⁵ Giessen University of Applied Sciences (THM), Institute of Mechanics and Materials,
Wiesenstr. 14, 35390 Giessen, Germany

^a Corresponding Author: vogler@isd.uni-hannover.de

Abstract:

A transversely isotropic elastic-viscoplastic constitutive law with a novel 3D failure criterion is presented, addressing high pressure effects, strain rate sensitivity in yielding and failure and volumetric plastic strain. The constitutive equations are derived in the framework of transversely-isotropic invariants, which allow for a coordinate system independent formulation and an easy parameter identification. Triaxiality dependent non-linearities are taken into account and entirely different yielding behavior under uniaxial/biaxial compression, uniaxial/biaxial tension and under in-plane/transverse shear stress states is addressed. Hardening curves for each loading state can easily be input either via tabulated data or optionally by use of a three parameter power law. Lateral plastic straining due to volumetric plastic compression and dilatation is load path dependent as well. In order to control the lateral plastic straining in each stress state, a non-associated flow rule, assuming a plastic potential which gives the direction of the plastic flow is introduced. The applicability of this novel material law is shown by two examples. The first one is a short fiber reinforced thermoplastic PA6GF60, the second one addresses off-axis tensile

and compression tests of a unidirectional carbon-epoxy IM7-8552, which is widely used in aircraft industry. For PA6GF60, a complete test setup for characterizing the novel transversely isotropic yield surface is used for validation. All test cases are simulated and compared with these experiments. The sensitivity of the plastic Poisson coefficient and the influence on the simulated load displacement curves are discussed. Strain rate effects are obtained from dynamic uniaxial tensile tests and are considered by a viscoplastic approach. Unidirectional carbon-epoxy IM7-8552 reveal pronounced yielding under combined shear- compression loadings as it is observed in off-axis compression tests. Furthermore, the glass transition temperature of epoxy resin drops from above 200°C to operating temperature in the presence of high pressures. This results in a change of mechanical properties, effecting the elastic parameters as well as the yielding behavior. This change of mechanical properties and the pronounced non-linear behavior in the presence of high pressure due to matrix yielding can be modeled properly with this new approach.

Keywords: Fiber reinforced composite structures, constitutive modeling, failure, nonlocal damage, integrative simulation.

1 Introduction

In contrast to metals, thermoplastic materials in general exhibit a strong pressure dependent material behavior, which results in different yielding in uniaxial tension and compression, under shear and under biaxial loadings. Furthermore, the assumption of volume constancy during plastification does not hold for thermoplastic polymers. Especially in the tensile range (uniaxial and biaxial tensile stress states) this effect can't be neglected. An isotropic model which is capable to capture these effects is implemented as material no. 187 (SAMP-1) in LS-DYNA, see [3].

Due to reorientation of molecule chains and due to fiber reinforcements, most thermoplastics also exhibit anisotropic material behavior. This direction dependent behavior does not only affect the yielding behavior, but also the strain rate sensitivity. A material and failure model, targeting these effects, is summarized subsequently. A more detailed description of the model is given in [4] and [5].

2 Experiments and FE-models

Fig 1 gives an overview over the available experimental data.

Übersicht Grundlagenversuche kurzfaserverstärkte Polyamide bei Raumtemperatur (Anzahl auswertbarer Wiederholungen)				Versuch / Geschwindigkeit								
				Zug (Junginger)	Zug (Junginger)	Zug (Junginger)	Schub (Arcan)	Schub (Arcan)	Druck (DKI)	Biegung (Impetus)	Biegung (Impetus)	Biegung (Impetus)
				q.-s.	0,35 m/s	1,5 m/s	q.-s.	0,56 m/s	q.-s.	1,0 m/s	2,5 m/s	4,0 m/s
Werkstoff (Fasergehalt) / Konditionierungszustand / Faserorientierung	PA6GF30	trocken (0,09%)	längs	4	4	4	3	--	3	5	5	5
			quer	4	4	4	3	--	3	5	4	5
		konditioniert (2,44% nach DIN 1110)	längs	4	4	4	4	--	4	5	5	4
			quer	4	4	4	4	--	4	5	5	4
	PA6GF60	trocken (0,06%)	längs	4	3	4	3	--	3	5	5	5
			quer	4	4	4	3	--	3	4	5	5
		konditioniert (1,26% nach DIN 1110)	längs	4	4	4	4	5	4	4	5	5
			quer	4	4	4	5	4	4	5	5	5

Figure 1: Overview experimental data basis

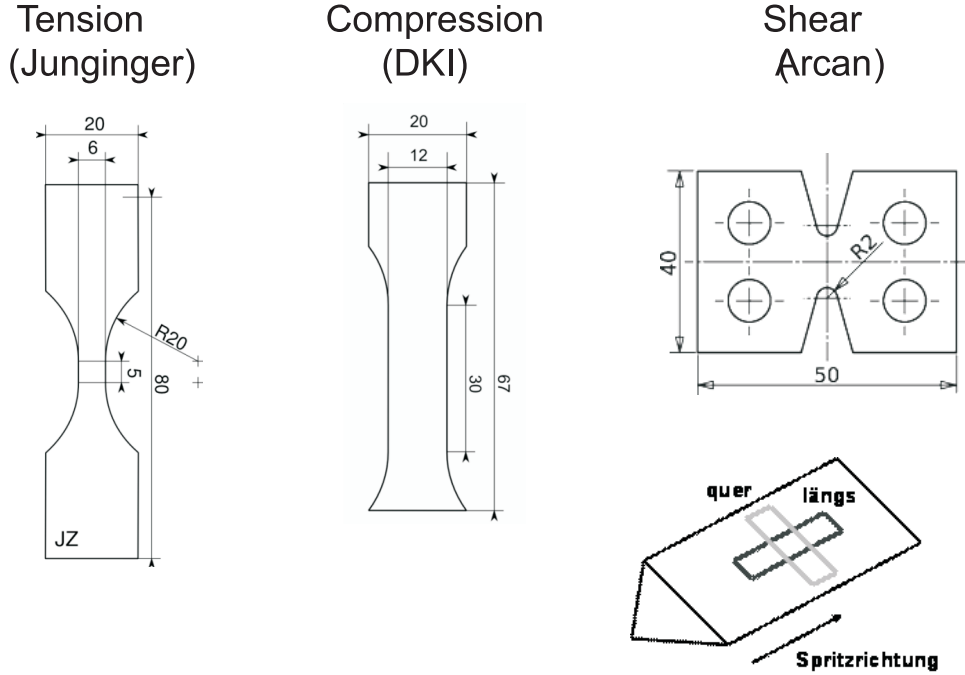


Figure 2: Geometry of specimen for tension, compression and shear

3 Constitutive Modeling

For establishing the constitutive equations for transverse isotropy, the mathematical framework of invariant theory is applied. This mathematical concept enables a representation of anisotropic constitutive functions as isotropic tensor functions. A profound description of the invariant theory is given in [7] and [8]. A detailed description of the invariant theory with respect to the construction of anisotropic yield functions and anisotropic constitutive equations in general is given in [9].

3.1 Yield surface formulation and definition of invariants

Transversely isotropic materials are characterized by a preferred direction \mathbf{a} . Thus, the material response is invariant with respect to arbitrary rotations around this preferred direction \mathbf{a} , to reflections at fiber parallel planes and with respect to the reflection at that plane, whose normal is \mathbf{a} . These are the group of symmetry transformations for transverse isotropy. The structural tensor \mathbf{A} of transverse isotropy, which represents the material's intrinsic characteristic, is defined as the dyadic product of the preferred direction \mathbf{a}

$$\mathbf{A} = \mathbf{a} \otimes \mathbf{a} \quad . \quad (1)$$

The structural tensor \mathbf{A} and the stress tensor $\boldsymbol{\sigma}$ are the argument tensors, whose isotropic invariants form the functional basis for constructing the yield function f as an isotropic tensor function

$$f = f(\boldsymbol{\sigma}, \mathbf{A}) \quad . \quad (2)$$

In accordance with the invariant theory, an arbitrary linear combination of the stress tensor $\boldsymbol{\sigma}$ can be used in Eq. 2. Hence, besides the stress tensor $\boldsymbol{\sigma}$ itself, the additional stress tensors $\boldsymbol{\sigma}^{\text{pind}}$ and $\boldsymbol{\sigma}^{\text{dev}}$ are used. The choice of stresses for constructing the invariants follows the target to identify certain stress states with corresponding invariants. Thus, the first two invariants I_1 and I_2 are composed of the stress tensor $\boldsymbol{\sigma}^{\text{pind}}$. This decomposition follows a proposal of Schroeder

$$\boldsymbol{\sigma} = \boldsymbol{\sigma}^{\text{pind}} + \boldsymbol{\sigma}^{\text{reac}} \quad , \quad (3)$$

with the stress components $\boldsymbol{\sigma}^{\text{reac}}$ and $\boldsymbol{\sigma}^{\text{pind}}$

$$\begin{aligned} \boldsymbol{\sigma}^{\text{reac}} &= \frac{1}{2}(\text{tr } \boldsymbol{\sigma} - \mathbf{a}\boldsymbol{\sigma}\mathbf{a})_p \mathbf{1} - \frac{1}{2}(\text{tr } \boldsymbol{\sigma} - 3\mathbf{a}\boldsymbol{\sigma}\mathbf{a})T_a \mathbf{A} \\ \boldsymbol{\sigma}^{\text{pind}} &= \boldsymbol{\sigma} - \frac{1}{2}(\text{tr } \boldsymbol{\sigma} - \mathbf{a}\boldsymbol{\sigma}\mathbf{a})\mathbf{1} + \frac{1}{2}(\text{tr } \boldsymbol{\sigma} - 3\mathbf{a}\boldsymbol{\sigma}\mathbf{a})\mathbf{A} \quad . \end{aligned} \quad (4)$$

and was originally developed for metal plasticity. The stress tensor $\boldsymbol{\sigma}^{\text{reac}}$ is called reaction stress tensor, because it contains the hydrostatic pressure and the projection of the stress tensor onto the preferred direction \mathbf{a} which are first assumed to not induce plastic yielding. The choice of using $\boldsymbol{\sigma}^{\text{pind}}$ instead of $\boldsymbol{\sigma}$ for constructing the invariants I_1 and I_2 enables to identify transverse shear loading solely with the invariant I_1 and in-plane shear loading solely with the invariant I_2 . Hence, a complete decoupling of the stress states with respect to their representation by invariants is achieved. This significantly simplifies the parameter identification. The definition of the invariants I_3 and I_4 is based on the same considerations. A decoupling of loadings into the preferred direction and transverse to the preferred direction should be achieved. The transversely isotropic invariants for establishing the yield surface are

$$\begin{aligned} I_1 &:= \frac{1}{2} \text{tr} (\boldsymbol{\sigma}^{\text{pind}})^2 - \mathbf{a} (\boldsymbol{\sigma}^{\text{pind}})^2 \mathbf{a} \quad , \\ I_2 &:= \mathbf{a} (\boldsymbol{\sigma}^{\text{pind}})^2 \mathbf{a} \quad , \\ I_3 &:= \text{tr } \boldsymbol{\sigma} - \mathbf{a}\boldsymbol{\sigma}\mathbf{a} \quad \text{and} \\ I_4 &:= \frac{3}{2} \mathbf{a}\boldsymbol{\sigma}^{\text{dev}} \mathbf{a} \quad , \end{aligned} \quad (5)$$

whereas the deviator of the stress tensor $\boldsymbol{\sigma}^{\text{dev}}$, used for constructing the fourth invariant I_4 , reads

$$\boldsymbol{\sigma}^{\text{dev}} = \boldsymbol{\sigma} - \frac{1}{3} \text{tr} \boldsymbol{\sigma} \mathbf{1} \quad . \quad (6)$$

With the invariants Eq. 5 in hand, the yield function as a function of the transversely-isotropic invariants reads

$$f = \alpha_1 I_1 + \alpha_2 I_2 + \alpha_3 I_3 + \alpha_{32} I_3^2 + \alpha_4 I_4 + \alpha_{42} I_4^2 - 1 \quad , \quad (7)$$

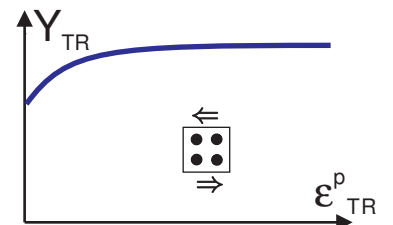
with 6 yield surface parameters α_1 , α_2 , α_3 , α_{32} , α_4 and α_{42} . Each of these parameters represent a certain loading state. The parameter α_1 stands for transverse shear, α_2 for in-plane shear, the parameters α_3 and α_{32} represent loading states transverse to the preferred direction and the parameters α_4 and α_{42} control yielding in fiber direction in compression and tension. In order to regard besides uniaxial stress states also biaxial tension and compression perpendicular to the fibers, a distinction is made, dividing the yield surface into a compressive part $I_3 < 0$ and a tensile part $I_3 > 0$. Following this, the parameters controlling yielding transverse to the preferred direction are denoted as α_3^c and α_{32}^c for the compressive range and α_3^t and α_{32}^t for the tensile range and the number of yield surface parameters increases from 6 (see Eq. 7) to 8. Consequently, 8 material tests are needed, giving the yield stress vs. the corresponding plastic strain for each loading. In particular, these are uniaxial tension and compression in fiber direction, uniaxial and biaxial tension in transverse direction, uniaxial and biaxial compression in transverse direction and in-plane and transverse shear. The hardening curves for each stress state can be feed directly via tabulated data into the LS-DYNA input deck.

3.2 Parameter Identification

The yield surface parameters are directly related to the current yield stress, given by the respective hardening curve for each stress state.

1. Transverse shear

$$\boldsymbol{\sigma} = \begin{bmatrix} 0 & Y_{TR} & 0 \\ Y_{TR} & 0 & 0 \\ 0 & 0 & 0 \end{bmatrix} , \quad \mathbf{a} = \begin{bmatrix} 0 \\ 0 \\ 1 \end{bmatrix}$$



$$I_1 = y_{tr}^2, \quad I_2 = 0, \quad I_3 = 0, \quad I_4 = 0$$

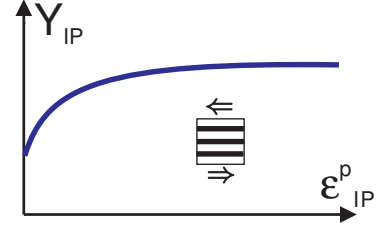
Inserting invariants into yield condition Eq. 7 gives:

$$f = \alpha_1 Y_{TR}^2 - 1 = 0 \quad (8)$$

$$\boxed{\alpha_1 := 1/Y_{TR}^2} \quad (9)$$

2. In-plane shear

$$\boldsymbol{\sigma} = \begin{bmatrix} 0 & Y_{IP} & 0 \\ Y_{IP} & 0 & 0 \\ 0 & 0 & 0 \end{bmatrix}, \quad \mathbf{a} = \begin{bmatrix} 1 \\ 0 \\ 0 \end{bmatrix}$$



$$I_1 = 0, \quad I_2 = Y_{IP}^2, \quad I_3 = 0, \quad I_4 = 0$$

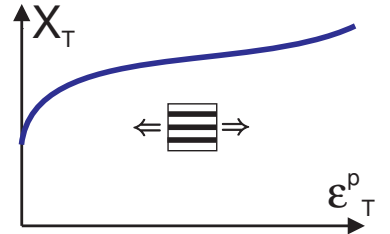
Inserting invariants into yield condition Eq. 7 gives:

$$f = \alpha_2 Y_{IP}^2 - 1 = 0 \quad (10)$$

$$\boxed{\alpha_2 := 1/Y_{IP}^2} \quad (11)$$

3. Tension in fiber direction

$$\boldsymbol{\sigma} = \begin{bmatrix} X_T & 0 & 0 \\ 0 & 0 & 0 \\ 0 & 0 & 0 \end{bmatrix}, \quad \mathbf{a} = \begin{bmatrix} 1 \\ 0 \\ 0 \end{bmatrix}$$

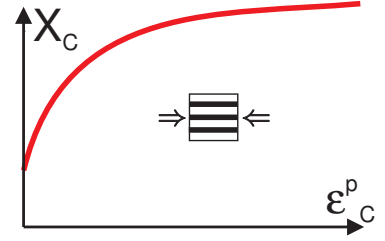


$$I_1 = 0, \quad I_2 = 0, \quad I_3 = 0, \quad I_4 = X_T$$

Inserting invariants into yield condition Eq. 7 gives:

$$\rightsquigarrow f = \alpha_4 X_T + \alpha_{42} X_T^2 - 1 = 0 \quad (12)$$

$$\boldsymbol{\sigma} = \begin{bmatrix} X_C & 0 & 0 \\ 0 & 0 & 0 \\ 0 & 0 & 0 \end{bmatrix}, \quad \mathbf{a} = \begin{bmatrix} 1 \\ 0 \\ 0 \end{bmatrix},$$



4. Compression in fiber direction

$$I_1 = 0, \quad I_2 = 0, \quad I_3 = 0, \quad I_4 = -X_C$$

Inserting invariants into yield condition Eq. 7 gives:

$$f = -\alpha_4 X_C + \alpha_{42} X_C^2 - 1 = 0 \quad (13)$$

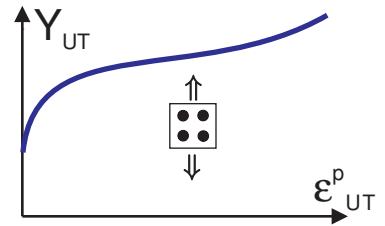
Eq. 16 and Eq. 17 are an equation system with the two unknowns α_4 and α_{42} , which can be easily solved :

$$\alpha_{42} := \frac{1 + \frac{X_T}{X_C}}{X_T^2 + X_C X_T} \quad (14)$$

$$\alpha_4 := \alpha_{42} X_C - \frac{1}{X_C} \quad (15)$$

5. Uniaxial tension transverse

$$\boldsymbol{\sigma} = \begin{bmatrix} 0 & 0 & 0 \\ 0 & 0 & 0 \\ 0 & 0 & Y_{UT} \end{bmatrix}, \quad \mathbf{a} = \begin{bmatrix} 1 \\ 0 \\ 0 \end{bmatrix}$$



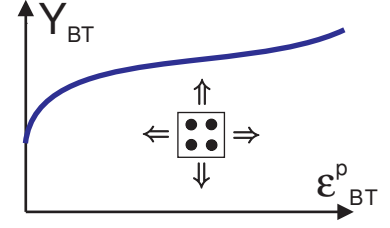
$$I_1 = \frac{Y_{UT}^2}{4}, \quad I_2 = 0, \quad I_3 = Y_{UT}, \quad I_4 = -\frac{Y_{UT}}{2}$$

Inserting invariants into yield condition Eq. 7 gives:

$$f = \alpha_1 \frac{Y_{UT}^2}{4} + \alpha_3^t Y_{UT} + \alpha_{32}^t (Y_{UT})^2 - \alpha_4 \frac{Y_{UT}}{2} + \alpha_{42} \frac{(Y_{UT})^2}{4} - 1 = 0 \quad (16)$$

6. Biaxial tension transverse

$$\boldsymbol{\sigma} = \begin{bmatrix} 0 & 0 & 0 \\ 0 & Y_{BT} & 0 \\ 0 & 0 & Y_{BT} \end{bmatrix}, \quad \mathbf{a} = \begin{bmatrix} 1 \\ 0 \\ 0 \end{bmatrix}$$



$$I_1 = 0, \quad I_2 = 0, \quad I_3 = 2Y_{BT}, \quad I_4 = -Y_{BT}$$

Inserting invariants into yield condition Eq. 7 gives:

$$f = 2\alpha_3^t Y_{BT} + 4\alpha_{32}^t (Y_{BT})^2 - \alpha_4 Y_{BT} + \alpha_{42} (Y_{BT})^2 - 1 = 0 \quad (17)$$

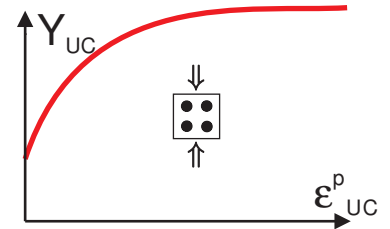
With parameters α_1 , α_4 and α_{42} in hand, Eq. 16 and Eq. 17 are an equation system with the two unknowns α_3^t and α_{32}^t , which can be easily solved :

$$\alpha_{32}^t := \frac{1 - \frac{Y_T}{2Y_{BT}} - \alpha_1 \frac{Y_T^2}{4} - \alpha_{42} \left(\frac{Y_T^2}{4} - \frac{Y_{BT}Y_T}{2} \right)}{Y_T^2 - 2Y_{BT}Y_T} \quad (18)$$

$$\alpha_3^t := \frac{1}{2Y_{BT}} - 2\alpha_{32}^t Y_{BT} + \alpha_4 \frac{1}{2} - \alpha_{42} \frac{Y_{BT}}{2} \quad (19)$$

7. Uniaxial compression transverse

$$\boldsymbol{\sigma} = \begin{bmatrix} 0 & 0 & 0 \\ 0 & 0 & 0 \\ 0 & 0 & Y_{UC} \end{bmatrix}, \quad \mathbf{a} = \begin{bmatrix} 1 \\ 0 \\ 0 \end{bmatrix}$$



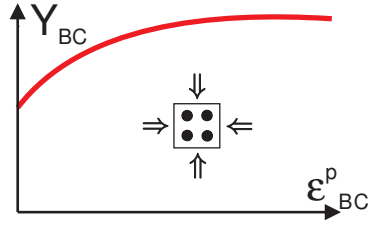
$$I_1 = \frac{(Y_{UC})^2}{4}, \quad I_2 = 0, \quad I_3 = -Y_{UC}, \quad I_4 = \frac{Y_{UC}}{2}$$

Inserting into yield condition Eq. 7 yields:

$$f = \alpha_1 \frac{(Y_{UC})^2}{4} - \alpha_3^c Y_{UC} + \alpha_{32}^c (Y_{UC})^2 + \alpha_4 \frac{Y_{UC}}{2} + \alpha_{42} \frac{(Y_{UC})^2}{4} - 1 = 0 \quad (20)$$

8. Biaxial compression transverse

$$I_1 = 0, \quad I_2 = 0, \quad I_3 = -2Y_{BC}, \quad I_4 = Y_{BC}$$

$$\boldsymbol{\sigma} = \begin{bmatrix} 0 & 0 & 0 \\ 0 & Y_{BC} & 0 \\ 0 & 0 & Y_{BT} \end{bmatrix}, \quad \mathbf{a} = \begin{bmatrix} 1 \\ 0 \\ 0 \end{bmatrix}$$


Inserting into yield condition Eq. 7 yields:

$$f = -2\alpha_3^c Y_{BC} + 4\alpha_{32}^c (Y_{BC})^2 + \alpha_4 Y_{BC} + \alpha_{42} (Y_{BC})^2 - 1 = 0 \quad (21)$$

With parameters α_1 , α_4 and α_{42} in hand, Eq. 20 and Eq. 21 are an equation system with the two unknowns α_3^c and α_{32}^c , which can be easily solved :

$$\alpha_{32}^c := \frac{1 - \frac{Y_T}{2Y_{BT}} - \alpha_1 \frac{Y_T^2}{4} - \alpha_{42} \left(\frac{Y_T^2}{4} - \frac{Y_{BT}Y_T}{2} \right)}{Y_T^2 - 2Y_{BT}Y_T} \quad (22)$$

$$\alpha_3^c := -\frac{1}{2Y_{BT}} + 2\alpha_{32}^c Y_{BT} + \alpha_4 \frac{1}{2} + \alpha_{42} \frac{Y_{BT}}{2} \quad (23)$$

Sometimes, not all material tests are available. In such cases, some tests described above can be replaced by off-axis tests. Furthermore, it is not easy to perform biaxial tests. In such cases, a reasonable behavior under biaxial stress states should be assumed by just scaling down the experimentally obtained uniaxial hardening curves. A typical material test, which is often delivered with material data, is a tensile test in direction of 45° to the fibers. For UD-material, off-axis tests can be performed much easier than transverse shear tests. Thus, a certain off-axis test 30° , 45° or 60° can replace a transverse shear test for instance. Illustrations of the yield surface can be done in stress space and invariant space. The invariant representation of yield and failure surface is a four dimensional surface. In order to illustrate the interaction of different loadings, various planes of the yield surface are chosen in Fig 3 and Fig 4 by setting the remaining invariants to zero. As each invariant can be associated with a certain stress state, a plot with two invariants gives an idea of interaction of different loading states. An illustration of the yield or failure surface in 3D or 2D stress space can be obtained by defining the vector \mathbf{a} of the preferred direction and the stress space itself (3D main stress space for instance). Each point in an arbitrary stress space has a unique representation in the four dimensional invariant space, however this does not work visa versa. Therefore, a scan of the stress

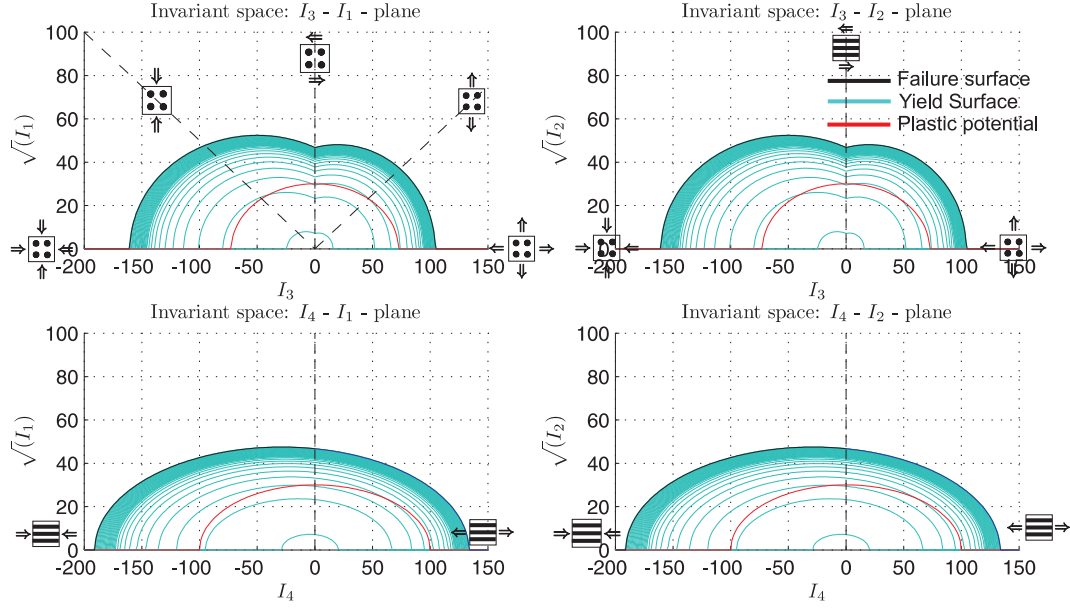


Figure 3: Yield surface, failure surface and plastic potential of PA6GF60 in invariant planes

space is performed by following load pathes and evaluating the yield condition in each point. If the yield condition is fulfilled, the respective point in stress space is marked. In Fig. 5 a plot of the failure surface for PA6GF60 is illustrated in $\sigma_{11} - \sigma_{22}$ -plane and in $\sigma_{22} - \sigma_{33}$ -plane.

3.3 Plastic potential and numerical treatment

In order to enable a realistic representation of plastic POISSON coefficients, a non-associated flow rule is applied. The plastic flow potential, which gives the direction of the projection onto the yield surface, is formulated as

$$g = \beta_1 I_1 + \beta_2 I_2 + \beta_3 I_3 + \beta_{32} I_3^2 + \beta_4 I_4^2 - 1 \quad . \quad (24)$$

The numerical treatment follows an elastic predictor plastic corrector scheme, assuming an additive decomposition of the strain increment. The stresses at the end of each time step t_{n+1} are

$$\sigma_{\mathbf{n}+1} = \sigma_{\mathbf{n}+1}^{\text{trial}} - \Delta \lambda_{\mathbf{n}+1} \mathbf{C}_e : \mathbf{m}_{\mathbf{n}+1} \quad , \quad (25)$$

whereas $\sigma_{\mathbf{n}+1}^{\text{trial}}$ are the elastic trial stresses, \mathbf{C}_e is the transversely isotropic elasticity tensor, $\Delta \lambda_{\mathbf{n}+1}$ is the sought plastic multiplier and $\mathbf{m}_{\mathbf{n}+1}$ is the direction of the plastic flow, given

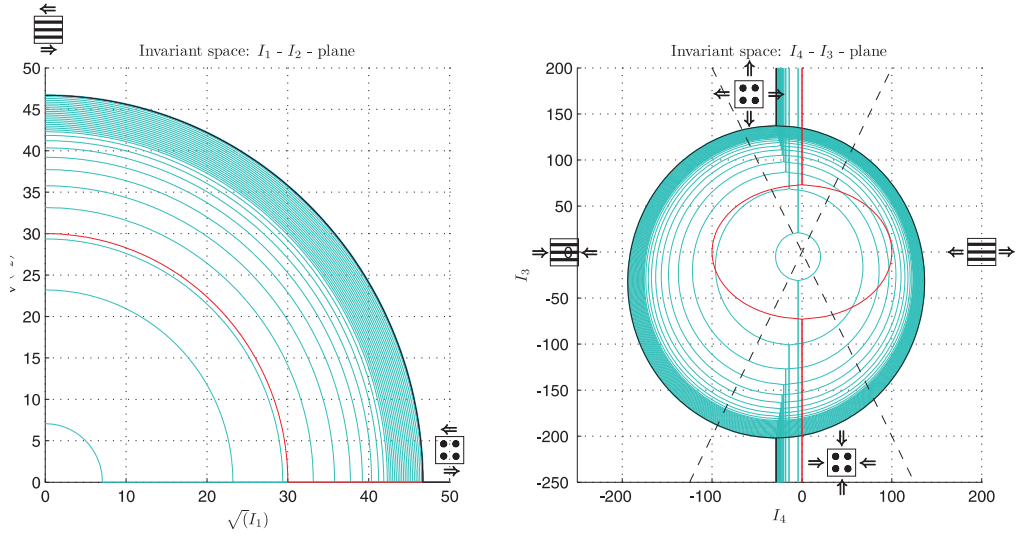


Figure 4: Yield surface, failure surface and plastic potential of PA6GF60 in invariant planes

by the plastic potential

$$\mathbf{m}_{n+1} = \partial g(\boldsymbol{\sigma}_{n+1}) / \partial \boldsymbol{\sigma}_{n+1} \quad . \quad (26)$$

Inserting the stresses $\boldsymbol{\sigma}_{n+1}$ into the yield surface formulation and enforcing the yield surface to be zero at the end of the time step (consistency condition $f_{n+1} = 0$) leads formally to a nonlinear equation in $\Delta\lambda_{n+1}$ which is solved by the Newton-Raphson method. With the plastic multiplier in hand, the plastic strains are updated at the end of each time step

$$\boldsymbol{\varepsilon}_{n+1} = \boldsymbol{\varepsilon}_n + \Delta\lambda_{n+1} \|\mathbf{m}_{n+1}\| \quad . \quad (27)$$

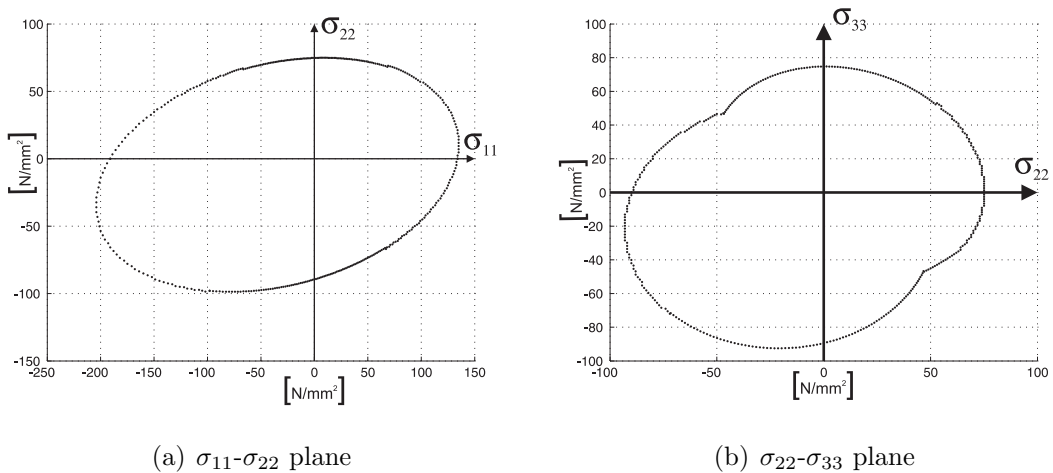


Figure 5: Failure surface of PA6GF60 in stress space

The derivations of the yield surface are:

$$\begin{aligned}
\partial_{\boldsymbol{\sigma}} f &= \partial_{I_i} f \partial_{\boldsymbol{\sigma}} I_i = \\
&\alpha_1 \boldsymbol{\sigma}^{\text{pind}} + (\alpha_2 - \alpha_1) (\mathbf{A} \boldsymbol{\sigma}^{\text{pind}} + \boldsymbol{\sigma}^{\text{pind}} \mathbf{A}) + \alpha_3 (\mathbf{1} - \mathbf{A}) \\
&+ 2\alpha_{32} I_3 (\mathbf{1} - \mathbf{A}) + \frac{3}{2} \alpha_4 \mathbf{A}^{\text{dev}} + 3\alpha_{42} I_4 \mathbf{A}^{\text{dev}} =: \mathbb{A} : \boldsymbol{\sigma} + \mathbf{B} \quad (28) \\
\partial_{\boldsymbol{\sigma}\boldsymbol{\sigma}}^2 f &= \alpha_1 \mathbb{P}^{\text{pind}} + (\alpha_2 - \alpha_1) \mathbb{P}_{\mathbf{A}}^{\text{pind}} + 2\alpha_{32} (\mathbf{1} - \mathbf{A}) \otimes (\mathbf{1} - \mathbf{A}) \\
&+ \frac{9}{2} \alpha_4 \mathbf{A}^{\text{dev}} \otimes \mathbf{A}^{\text{dev}} =: \mathbb{A}
\end{aligned}$$

with the projection tensors

$$\begin{aligned}
\mathbb{P}^{\text{pind}} &:= \partial_{\boldsymbol{\sigma}} \boldsymbol{\sigma}^{\text{pind}} = \mathbb{I} - \frac{1}{2} (\mathbf{1} \otimes \mathbf{1}) + \frac{1}{2} (\mathbf{A} \otimes \mathbf{1} + \mathbf{1} \otimes \mathbf{A}) - \frac{3}{2} (\mathbf{A} \otimes \mathbf{A}) \quad , \quad (29) \\
\mathbb{P}_{\mathbf{A}}^{\text{pind}} &= P_{\mathbf{A}}^{\text{pind}}{}_{ijkl} := A_{im} P_{m jkl}^{\text{pind}} + A_{mj} P_{i mkl}^{\text{pind}}
\end{aligned}$$

and \mathbf{A}^{dev} is the deviator of the structural tensor \mathbf{A} , \mathbb{A} is the constant bending tensor and \mathbf{B} is the first derivative of the linear terms in $\boldsymbol{\sigma}$ of the quadratic yield locus. This enables to state the yield function eq. (7) in the more general form

$$f = \frac{1}{2} \boldsymbol{\sigma} : \mathbb{A} : \boldsymbol{\sigma} + \mathbf{B} : \boldsymbol{\sigma} - 1 \quad . \quad (30)$$

In the same way, the plastic potential Eq. (24) reads in the more general form

$$g = \frac{1}{2} \boldsymbol{\sigma} : \mathbb{H} : \boldsymbol{\sigma} + \mathbf{K} : \boldsymbol{\sigma} - 1 \quad . \quad (31)$$

It should be noted, that the well known Hill yield criterion is comprised as a special case in the given yield surface formulation.

3.4 Failure criterion and nonlocal damage formulation

The failure surface follows the same equation as the yield surface formulation, see Eq. 7. Therefore, the experimentally identified ultimate strengthes in each loading state are required for calculating the six failure surface parameters in Eq. 7. In particular these are the fiber parallel strengthes in tension and compression, R_{\parallel}^t and R_{\parallel}^c , the uniaxial tensile and compressive strength perpendicular to the fiber direction, R_{\perp}^t and R_{\perp}^c , and the material strength of transverse shear $R_{\perp\perp}$ and in-plane shear $R_{\parallel\perp}$. If the failure criterion is active, a degradation of the stresses is performed using a nonlocal damage approach, following a proposal of [1]. Whenever strain-softening is present, the results are inevitably pathologically mesh dependent if the local continuum theory is considered. This very often

leads to nonphysical results in the simulation of material failure, significantly diminishing the quality and accuracy of numerical predictions.

In order to avoid mesh-dependent solutions, we shall adopt herein an approximation of the nonlocal theory that is especially suitable for implementation in explicit finite element codes as discussed in references [1, 2]. Adopting this particular regularization scheme, the updated value of damage, d , is defined as a linear function of the nonlocal equivalent strain, $\bar{\varepsilon}_{n+1}^p$, that is,

$$d(\bar{\varepsilon}_{n+1}^p) = \alpha(\bar{\varepsilon}_{n+1}^p - \varepsilon_{fail}^p) \quad (32)$$

where

$$\bar{\varepsilon}_{n+1}^p = \frac{\bar{\varepsilon}_n^p}{\varepsilon_n^p} \varepsilon_{n+1}^p \quad (33)$$

In the equation above, $\bar{\varepsilon}_n^p$ corresponds to the nonlocal average of the strain tensor norm, evaluated using the values of the local strain norm, ε^p , from the *previous* timestep. For the sake of readability, we shall omit the details concerning the nonlocal technique and the reader is referred to reference [2] which clarifies the employed nonlocal strategy in detail. Nonetheless, it is worth mentioning that the present nonlocal technique has been straightforwardly coupled with the constitutive model presented in this paper, requiring only minor modifications in the original (local) LS-DYNA material routine.

4 Results

4.1 Short fiber reinforced thermoplastic PA6GF60

Simulation results for PA6GF60 are shown in Fig. 6. Different yielding and failure under tension/compression transverse, under tension/compression longitudinal and under shear is simulated with just one parameter set. There is no need of time consuming parameter fitting, the experimentally obtained stress strain curves are feed into the material law via tabulated data. In Fig. 7 the regularizing effect on the localization of damage due to the nonlocal damage approach is illustrated. A detailed description of the nonlocal framework is given in [2].

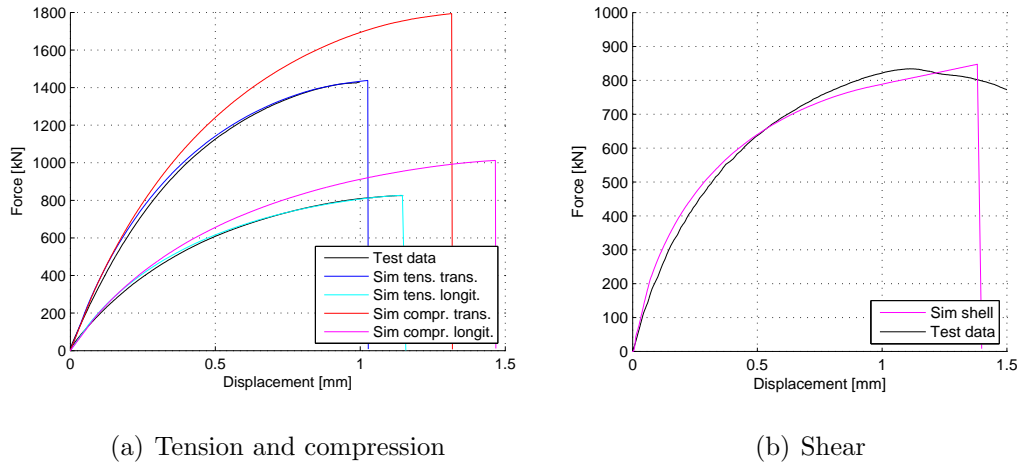


Figure 6: Simulation results PA6GF60, different yielding behavior in compression and tension transverse and longitudinal and under shear loading

4.2 Quasistatic and dynamic off-axis compression tests IM7-8552

Fig. 9 shows the simulation results of quasi-static and dynamic off-axis tests. The test data are taken from [10]. Both the non-linear material behavior and the onset of failure can be described very well with the novel 3D material and failure model presented. The experiments [10] show, that there are quite homogenous stress and strain field during load application. Just immediately before final failure occurs, localization in the fracture plane, resp. in the kink plane (15° off-axis test) is observed. Also this effect can be simulated with the combined continuum approach and failure criterium.

References

- [1] J.M.A. Cesar de Sa, F.X.C. Andrade and F.M. Andrade Pires: Theoretical and Numerical Issues on Ductile Failure Prediction - An Overview. *Computer Methods in Materials Science*, v. 10, No. 4, pp. 279–293, 2010.
- [2] F.X.C. Andrade, M. Vogler, J.M.A. Cesar de Sa and F.M. Andrade Pires: User-Defined Nonlocal Models in LS-DYNA. In *7th European LS-DYNA Users Conference*, Strasbourg, 2011.

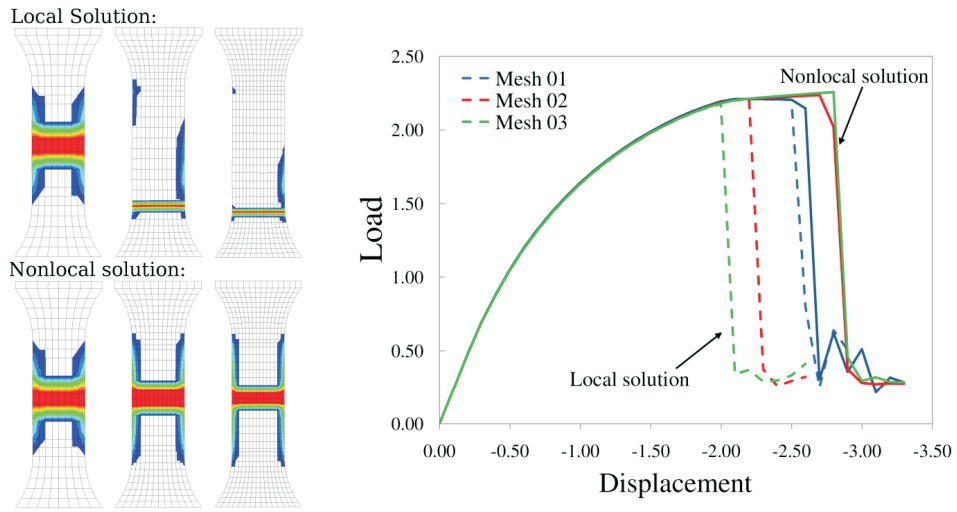


Figure 7: Results compression specimen: damage contour and Force-displacement diagram

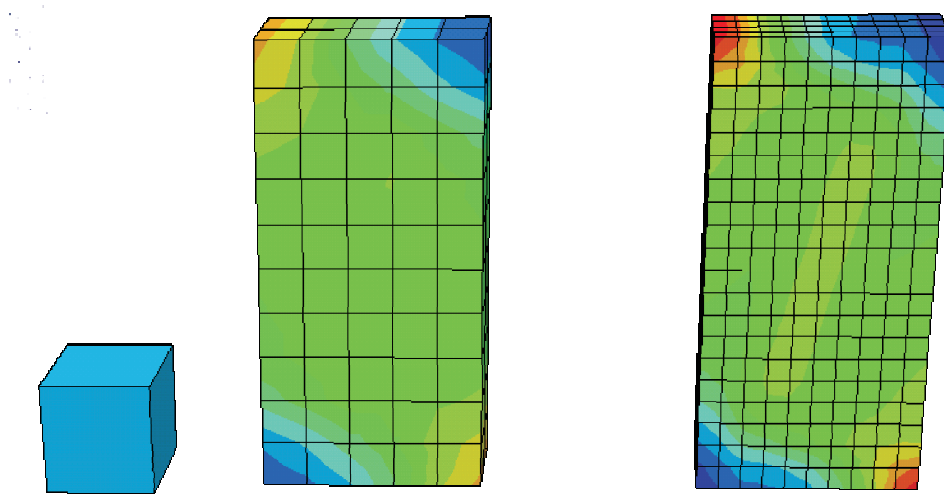


Figure 8: FE mesh for off-axis compression tests: single cube, coarse and medium mesh

- [3] S. Kolling, A. Haufe, M. Feucht, P.A. Du Bois. A semianalytical model for the simulation of polymers. *Proceedings of the 4th LS-DYNA Forum, Bamberg, Germany, A-II:27–52*, 2005.
- [4] M. Vogler, R. Rolfes, S. Kolling. Orthotropic plasticity with application to fibre-reinforced thermoplastics. *Proceedings of the 6th LS-DYNA Forum Meeting, Frankfurt, Germany, D-II:55–74*, 2007.
- [5] M. Vogler, G. Ernst and R. Rolfes: Invariant based transversely-isotropic material

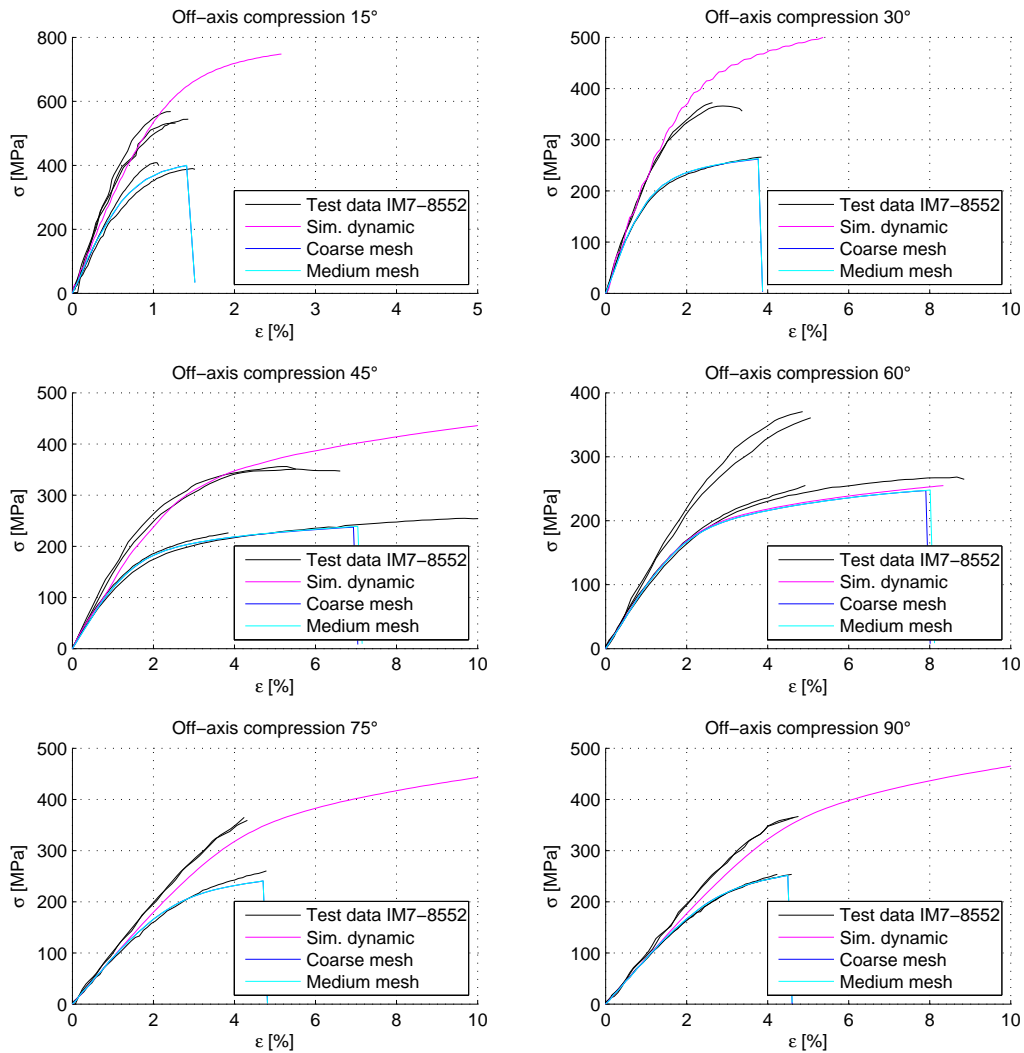


Figure 9: Results Off-axis compression tests unidirectional carbon-epoxy IM7-8552

and failure model for fiber-reinforced polymers. *CMC: Computers, Materials, & Continua*, Vol. 16, No. 1, pp. 25-50, 2010

- [6] M. Vogler, F.X.C. Andrade, J. Schöpfer, S. Kolling, R. Rolfes: A novel transversely-isotropic 3D elastic-viscoplastic constitutive law for modeling fiber matrix composites. In *8th European LS-DYNA Users Conference*, Strasbourg, 2011.
- [7] Boehler, J.P.: Applications of Tensor Functions in Solid Mechanics. CISM No. 292, Springer, 1987.

- [8] Spencer, A.J.M.: Kinematic Constraints, Constitutive Equations and Failure Rules for Anisotropic Materials. In: Applications of Tensor Functions in Solid Mechanics, Ed.: Boehler, J.P., CISM No. 292, S. 187-201, Springer, 1987.
- [9] Schröder, J.: Theoretische und algorithmische Konzepte zur phänomenologischen Beschreibung anisotropen Materialverhaltens. Dissertation, Universität Hannover (1995)
- [10] H. Koerber, J. Xavier, P.P. Camanho: High strain rate characterisation of unidirectional carbon-epoxy IM7-8552 in transverse compression and in-plane shear using digital image correlation, Mechanics of Materials, Volume 42, Issue 11, November 2010, Pages 1004-1019